Functional Characterization of the Type 1 Inositol 1,4,5-Trisphosphate Receptor Coupling Domain SII(±) Splice Variants and the *Opisthotonos* Mutant Form

Huiping Tu,* Tomoya Miyakawa,[†] Zhengnan Wang,* Lyuba Glouchankova,* Masamitsu Iino,[†] and Ilya Bezprozvanny*

*Department of Physiology, University of Texas Southwestern Medical Center at Dallas, Dallas, Texas 75390 USA and
[†]Department of Pharmacology, Graduate School of Medicine, The University of Tokyo, Tokyo 113-0033, Japan

ABSTRACT   The type 1 inositol (1,4,5)-trisphosphate receptor (InsP$_3$R1) plays a critical role in Ca^{2+} signaling in cells. Neuronal and nonneuronal isoforms of the InsP$_3$R1 differ by alternative splicing in the coupling domain of the InsP$_3$R1 (SII site) (Danoff et al., 1991). Deletion of 107 amino acids from the coupling domain of the InsP$_3$R1 results in epileptic-like behaviors in *opisthotonos* (*opt*) spontaneous mouse mutant (Street et al., 1997). Using *Spodoptera frugiperda* cells expression system, we compared single-channel behavior of recombinant InsP$_3$R1-SII(+), InsP$_3$R1-SII(−), and InsP$_3$R1-*opt* channels in planar lipid bilayers. The main results of our study are: 1) the InsP$_3$R1-SII(−) has a higher conductance (94 pS) and the InsP$_3$R1-*opt* has a lower conductance (64 pS) than the InsP$_3$R1-SII(+) (81 pS); 2) the bell-shaped Ca^{2+}-dependence peaks at 200–300 nM Ca^{2+} for all three InsP$_3$R1 isoforms; 3) the bell-shaped Ca^{2+}-dependence is wider for the InsP$_3$R1-SII(+) and narrower for the InsP$_3$R1-SII(−) and InsP$_3$R1-*opt*; 4) the apparent affinity for ATP is sixfold lower for the InsP$_3$R1-SII(−) (1.4 mM) and 20-fold lower for the InsP$_3$R1-*opt* (5.3 mM) than for the InsP$_3$R1-SII(+) (0.24 mM); 5) the InsP$_3$R1-SII(−) is approximately twofold more active than the InsP$_3$R1-SII(+) in the absence of ATP. Obtained results provide novel information about the molecular determinants of the InsP$_3$R1 function.

INTRODUCTION

The inositol (1,4,5)-trisphosphate receptor (InsP$_3$R) is an intracellular calcium (Ca^{2+}) release channel that plays an important role in Ca^{2+} signaling in cells (Berridge, 1993). Three mammalian isoforms of the InsP$_3$R share 60–70% amino acid homology and differ in tissue distribution (Furuichi et al., 1994). The type 1 receptor (InsP$_3$R1) is a predominant neuronal isoform that plays an important role in brain function (Matsumoto et al., 1996) and contributes to synaptic plasticity (Fujii et al., 2000; Itoh et al., 2001). The InsP$_3$R plays a central role in signal transduction and is subjected to multiple levels of regulation (Berridge, 1993; Bezprozvanny and Ehrlich, 1995; Ferris and Snyder, 1992b; Furuichi et al., 1994; Taylor, 1998). Binding of InsP$_3$ triggers the InsP$_3$R channel opening. The activity of InsP$_3$R1 is biphasically modulated by cytosolic Ca^{2+} (Bezprozvanny et al., 1991; Finch et al., 1991; Iino, 1990; Kaznacheyeva et al., 1998; Ramos-Franco et al., 1998b) and allosterically potentiated by adenine nucleotides (Bezprozvanny and Ehrlich, 1993; Ferris et al., 1990; Iino, 1991). The InsP$_3$R1 is also phosphorylated by protein kinase A (PKA), protein kinase C (PKC), and Ca^{2+}/calmodulin (CaM)-kinase (Ferris et al., 1991b; Supattapone et al., 1988; Yamamoto et al., 1989) with resulting changes in the InsP$_3$R1 function (Cam-

eron et al., 1995; Nakade et al., 1994; Supattapone et al., 1988).

The functional InsP$_3$R channel is a tetrameric complex (Maeda et al., 1991; Mignery et al., 1989). Each InsP$_3$R subunit consists of three distinct domains (Mignery and Sudhof, 1990; Miyawaki et al., 1991): the carboxy-terminal Ca^{2+} channel domain; the amino-terminal ligand binding domain; and the middle coupling domain. A number of putative modulatory sites (phosphorylation sites, ATP binding sites, calmodulin binding site, Ca^{2+}-binding sites) are located in the coupling domain of the InsP$_3$R1 (Furuichi et al., 1994). The SII site of alternative splicing is also located in this region (Furuichi et al., 1994). The predominant neuronal isoform of InsP$_3$R1 is SII(+) and nonneuronal isoform is SII(−) (Danoff et al., 1991; Nakagawa et al., 1991a, 1991b). The excision of the SII insert changes the PKA phosphorylation pattern of the InsP$_3$R1 (Danoff et al., 1991; Ferris et al., 1991a) and creates additional ATP (Ferris and Snyder, 1992b) and CaM (Islam et al., 1996; Lin et al., 2000) binding sites in the InsP$_3$R1 sequence.

The autosomal recessive *opisthotonos* (*opt*) is a spontaneous mouse mutation resulting in epileptic-like behaviors, similar to the phenotype of InsP$_3$R1 knockout mice (Matsumoto et al., 1996). The seizures in *opt* homozygotes begin at 14 days postnatal and become progressively more severe, leading to death at 3–4 weeks of age. Recent genetic analysis of the *opt* mutant identified a >10-kilobase (kb) deletion within the InsP$_3$R1 gene (Street et al., 1997). As a result of this deletion, a fragment of 107 amino acids, containing several putative regulatory sites, is removed from the InsP$_3$R1 coupling region in the *opt* mice (Street et al., 1997).

Alterations in the InsP$_3$R1 properties caused by the *opt* mutation have not been previously described.

Here we analyzed single-channel behavior of the InsP$_3$R1-SII(+), InsP$_3$R1-SII(−), and InsP$_3$R1-*opt* channels in identical experimental conditions. The recombinant InsP$_3$R1 for these studies were expressed in insect *Spodoptera frugiperda* (Sf9) cells using a baculovirus expression system. Microsomes isolated from the InsP$_3$R1-expressing Sf9 cells were fused to planar lipid bilayers, and activity of the InsP$_3$R1 was analyzed at the single channel level. Obtained results provided novel information about molecular determinants of the InsP$_3$R1 function.

MATERIALS AND METHODS

Generation of recombinant baculoviruses

The full-length neuronal rat InsP$_3$R1 (SI−/SII+) (Mignery et al., 1990) expression construct in pcDNA3 vector was previously described (Kaznacheyeva et al., 1998). The coding sequence of the InsP$_3$R1-SII(+) was excised from pcDNA3 vector with *Xho*I and *Xba*I and subcloned into *Sal*I and *Xba*I sites of pFastBac1 expression vector (Invitrogen Corp, Carlsbad, CA). Generated pFastBac1-InsP$_3$R1-SII(+) plasmid was transformed into DH10Bac (Invitrogen) *Escherichia coli* strain, and baculoviruses expressing InsP$_3$R1 were generated using Bac-to-Bac baculovirus expression system according to manufacturer's (Invitrogen) protocol. Generated RT1 (InsP$_3$R1-SII(+)) baculoviruses were amplified three times to yield P3 stock with the titer 10^8-10^9 pfu/ml. InsP$_3$R1-SII(−) (deletion of amino acids Q1692-R1731) and InsP$_3$R1-*opt* (deletion of amino acids G1732-Q1839) mutations were introduced by inverse polymerase chain reaction and verified by sequencing. The 2.5-kb fragments of InsP$_3$R1 sequence containing the SII(−) spliced region or the *opt* mutation were subcloned into pFastBac1-InsP$_3$R1 and the recombinant baculoviruses SII(−) (InsP$_3$R1-SII(−)) and *opt* (InsP$_3$R1-*opt*) were generated and amplified using Bac-to-Bac system (Invitrogen).

Expression of the InsP$_3$R1 in Sf9 cells

Sf9 cells were obtained from American Type Culture Collection (Manassas, VA) and cultured in suspension culture in supplemented Grace's insect media (Invitrogen) with 10% fetal bovine serum at 27°C. For the InsP$_3$R1 expression, 150 ml of Sf9 cell culture was infected by InsP$_3$R1-encoding baculovirus at 5–10 multiplicity of infection (MOI). 66 h post-infection, Sf9 cells were collected by centrifugation at 4°C for 5 min at 800 rpm (GH 3.8 rotor, Beckman Instruments, Fullerton, CA). The cellular pellet was resuspended in 25 ml of homogenization buffer (sucrose 0.25 M, Hepes 5 mM, pH 7.4) supplemented with protease inhibitors cocktail (1mM ethylenediaminetetraacetic acid, aprotinin 2 μg/ml, leupeptin 10 μg/ml, benzamidine 1 mM, 4-(2-aminoethyl)benzenesulfonyl fluoride hydrochloride 2.2 mM, pepstatin 10 μg/ml, phenylmethyl sulfonyl fluoride 0.1 mg/ml). Cells were disrupted by sonication (Branson Ultrasonics, Danbury, CT) and manually homogenized on ice with a glass-Teflon (DuPont, Wilmington, DE) homogenizer. The microsomes were isolated from the Sf9 cell homogenate by gradient centrifugation as previously described for human embryonic kidnet (HEK)-293 cells (Kaznacheyeva et al., 1998). The final microsomal preparation was resuspended in 0.5 ml of the storage buffer (10% sucrose, 10 mM 3-(N-Morpholino)propanesulfonic acid pH 7.0) to typically yield 6 mg/ml of protein (Bradford assay, Bio-Rad, Hercules, CA), aliquoted, quickly frozen in liquid nitrogen, and stored at −80°C. Expression of the InsP$_3$R1 was confirmed by Western blotting using the anti-InsP$_3$R1 rabbit polyclonal antibody that was previously described (Kaznacheyeva et al., 1998).

Single-channel recordings and analysis of the InsP$_3$R1 activity

Recombinant InsP$_3$R1 expressed in Sf9 cells were incorporated into the bilayer by microsomal vesicle fusion as described previously for native cerebellar InsP$_3$R and for the InsP$_3$R1 expressed in HEK-293 cells (Bezprozvanny and Ehrlich, 1993, 1994; Bezprozvanny et al., 1991; Kaznacheyeva et al., 1998). Single-channel currents were recorded using 50 mM Ba^{2+} dissolved in Hepes (pH 7.35) in the *trans* (intraluminal) side as a charge carrier (Bezprozvanny and Ehrlich, 1994). Transmembrane potential during current recordings was fixed to 0 mV in Ca^{2+}- and ATP-dependence experiments, and varied between +10 mV and −30 mV in current-voltage relationship experiments. The *cis* (cytosolic) chamber contained 110 mM Tris dissolved in Hepes (pH 7.35). To obtain Ca^{2+}-dependence of the InsP$_3$R1, we followed the protocol from Bezprozvanny et al. (1991). Free Ca^{2+} concentration in the *cis* chamber was controlled in the range of 10 nM (pCa 8) to 10 μM (pCa 5) by a mixture of 1 mM EGTA, 1 mM *N*-(2-hydroxyethyl)ethylenediamine-*N,N′,N′*-triacetic acid, and variable concentrations of CaCl$_2$. The resulting free Ca^{2+} concentration was calculated by using a program described in Fabiato (1988). ATP-dependence of InsP$_3$R1 was measured by consecutive addition of Na$_2$ATP to the *cis* chamber from 100 mM stock. All additions (InsP$_3$, ATP, CaCl$_2$) were to the *cis* chamber from the concentrated stocks with at least 30 s of stirring solutions in both chambers. InsP$_3$R1 single-channel currents were amplified (Warner OC-725, Warner Instruments Corp, Hamden, CT), filtered at 1 kHz by low-pass 8-pole Bessel filter, digitized at 5 kHz (Digidata 1200, Axon Instruments, Union City, CA) and stored on a computer hard drive and recordable optical discs.

For off-line computer analysis (pClamp 6, Axon Instruments) single-channel data were filtered digitally at 500 Hz; for presentation of the current traces, data were filtered at 200 Hz. Evidence for the presence of 2–3 functional channels in the bilayer was obtained in majority of the experiments. The number of active channels in the bilayer was estimated as a maximal number of simultaneously open channels during the course of an experiment (Horn, 1991). The open probability of closed level, and 1st and 2nd open levels was determined by using half-threshold crossing criteria ($t \geq 2$ ms) from the records lasting at least 2.5 min. The single-channel open probability (*Po*) for one channel was calculated using the binomial distribution for the levels 0, 1, and 2, and assuming that the channels were identical and independent (Colquhoun and Hawkes, 1995). In analysis of Ca^{2+}- and ATP-dependence experiments, potential errors in absolute *Po* values were minimized by normalizing the *Po* to the maximum *Po* observed in the same experiment.

Ca^{2+} imaging in DT40 cells

DT40 chicken B lymphoma cells were cultured in RPMI1640 supplemented with 10% fetal calf serum, 1% chicken serum, penicillin (100 U/ml), streptomycin (100 U/ml), and 2 mM glutamine. Mutant DT40 cells with all three of their InsP$_3$R genes disrupted (Sugawara et al., 1997) were transfected with the linearized rat pcDNA3-InsP$_3$R1-SII(+), pcDNA3-InsP$_3$R1-SII(−), and pcDNA3-InsP$_3$R1-*opt* plasmids by electroporation (330 V, 250 μF). Several stably expressing clones were isolated in the presence of 2 mg/ml G418 (Geneticin, Invitrogen). Ca^{2+} imaging of the InsP$_3$R1-SII(+), InsP$_3$R1-SII(−), and InsP$_3$R1-*opt* transfected cells was performed as described previously (Miyakawa et al., 1999, 2001). Briefly, cells on poly-L-lysine and collagen-coated coverslips were loaded with 1 μM Fura-2AM. The fluorescence images were captured at room temperature (22–24°C) with an Olympus IX70 inverted microscope, equipped with a cooled charge-coupled device camera (Photometrics, Tucson, AZ) and a polychromatic illumination system (T.I.L.L. Photonics, Germany) at a rate of one pair of frames with excitation at 345 and 380 nm every 10, 1, or 0.25 s. Intracellular Ca^{2+} concentrations of the Fura-2-loaded cells were calculated using the equation reported previously (Grynkiewicz et al., 1985).
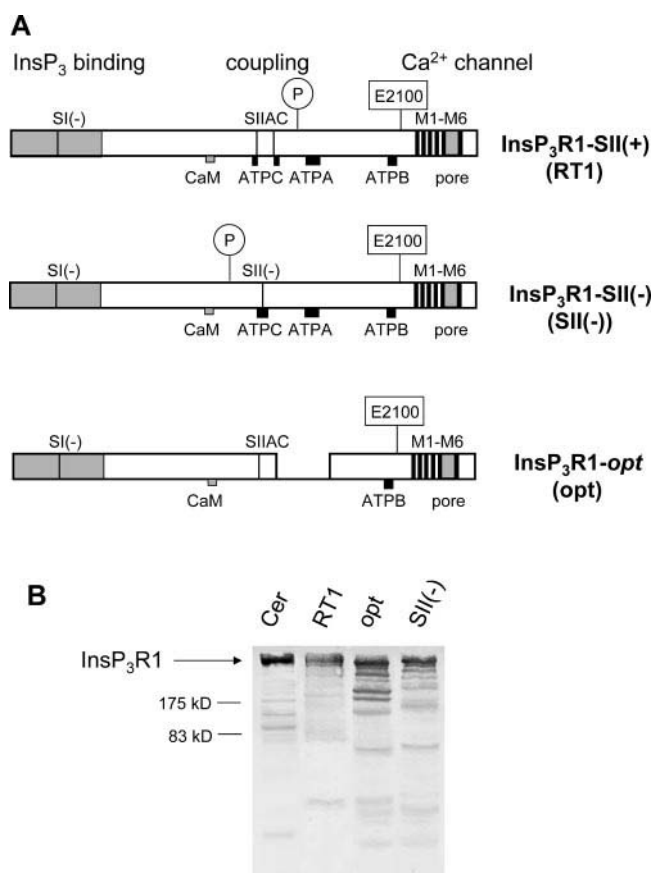
FIGURE 1 Structure and expression of the InsP$_3$R1-SII(+) (RT1), InsP$_3$R1-SII(−) (SII(−)), and InsP$_3$R1-*opt* (opt) isoforms. (*A*) Diagram of rat InsP$_3$R1-SII(+), InsP$_3$R1-SII(−), and InsP$_3$R1-*opt* constructs used in this study. The domain structure of the InsP$_3$R1, ATP-binding sites, CaM-binding site, transmembrane domains, and the Ca^{2+} channel pore region are adapted from Furuichi et al. (1994). The preferential sites of PKA phosphorylation (S1589 for SII(−) and S1755 for SII(+)) are from Danoff et al. (1991) and Ferris et al. (1991a). PKA phosphorylation pattern of the InsP$_3$R1-*opt* mutant is not known. The E2100 residue was recently identified as part of the InsP$_3$R1 activating Ca^{2+} sensor (Miyakawa et al., 2001). (*B*) Western blot of microsomal proteins. Rat cerebellum microsomes (cer) and microsomes isolated from Sf9 cells infected with RT1, SII(−), and *opt* baculoviruses were analyzed by Western blotting with anti-InsP$_3$R1 polyclonal antibody. For each microsomal preparation, 20 μg of total protein was loaded on the gel.

RESULTS

Functional expression of the InsP$_3$R1-SII(±) splice variants and the InsP$_3$R1-*opt* mutant

To study the properties of recombinant InsP$_3$R1, we generated baculovirus encoding rat InsP$_3$R1-SII(+) (RT1), InsP$_3$R1-SII(−) (SII(−)), and InsP$_3$R1-*opt* (opt) as described in Methods. The SII splicing region of InsP$_3$R1 is 40 amino acids long and can be further subdivided into A, B, and C regions (Nakagawa et al., 1991a, 1991b). The sequence of InsP$_3$R1-SII(+) (Mignery et al., 1990) (Fig. 1 *A*) corresponds to the SIIAC isoform, a major cerebellar iso-

form of the InsP$_3$R1 (Nakagawa et al., 1991a, 1991b). The sequence of InsP$_3$R1-SII(−) (Fig. 1 *A*) corresponds to SIIABC(−) isoform (deletion of Q1692-R1731) expressed in peripheral tissues (Danoff et al., 1991; Nakagawa et al., 1991a, 1991b). Genomic deletion in the *opt* mutant results in removal of two exons immediately after the SII region of alternative splicing (Street et al., 1997). As a result of alternative splicing in the SIIABC region, four possible InsP$_3$R1 mRNAs are expressed in brains of *opt* homozygotes (Street et al., 1997). In this paper we re-created the *opt* mutation (deletion of G1732-Q1839) on the basis of InsP$_3$R1-SIIAC isoform (Fig. 1 *A*).

Microsomes isolated from the RT1, SII(−) and *opt*-infected Sf9 cells, but not from noninfected cells, contained large quantities of the InsP$_3$R1 detectable by Western blotting (Fig. 1 *B*). Small amounts of endogenous InsP$_3$R1 were detected in microsomes from noninfected Sf9 cells when the blots were overexposed (data not shown). The apparent molecular size of recombinant InsP$_3$R1-SII(+) was identical to the InsP$_3$R1 present in rat cerebellar microsomes (Fig. 1 *B*). The predicted molecular weights are 311,401 Da for the InsP$_3$R1-SII(+), 306,939 Da for the InsP$_3$R1-SII(−), and 300,299 Da for the InsP$_3$R1-*opt*. Relatively small size differences among the InsP$_3$R1-SII(+) and the InsP$_3$R1-SII(−) (1.4%) or the InsP$_3$R1-*opt* (3.6%) isoforms could not be reliably resolved on the 8% acrylamide gel used in our experiments. The shorter molecular size products detected by anti-InsP$_3$R1 antibodies in all four samples (Fig. 1 *B*) correspond to partial degradation products of the InsP$_3$R1 resulting from the limited proteolysis during microsomal extraction or isolation procedure. From the relative abundance of degradation products on the gel, it seems that the InsP$_3$R1-*opt* mutant is more sensitive to proteolysis than the wild type SII(+) or SII(−) isoforms (Fig. 1 *B*). It is possible that the increased sensitivity of InsP$_3$R1-*opt* mutant to proteolysis contributed to 10-fold reduction in the level of the InsP$_3$R1 protein in the brain of the *opt* mutant mice (Street et al., 1997).

When microsomes isolated from the RT1-infected Sf9 cells were fused with planar lipid bilayers, InsP$_3$-gated channels were frequently (in 30 of 40 experiments) observed (Fig. 2). In contrast, the InsP$_3$-gated channels were never (n = 10) observed in experiments with microsomes from noninfected cells. Therefore, we concluded that channels observed in our planar lipid bilayer experiments with microsomes from the RT1-infected Sf9 cells correspond to the activity of recombinant rat InsP$_3$R1. The InsP$_3$R1 plasmid used to generate RT1 baculovirus corresponds to a major cerbellar isoform SIIAC (Fig. 1 *A*). As expected, the gating and conductance properties of channels observed in experiments from RT1-infected Sf9 cells were identical to the native channels observed in experiments with rat cerebellar microsomes (Fig. 2). To determine the functional properties of the InsP$_3$R1-SII(−) splice variant and the

FIGURE 2 Single-channel records of native rat cerebellar InsP$_3$R, recombinant InsP$_3$R1-SII(+), InsP$_3$R1-*opt*, and InsP$_3$R1-SII(−) isoforms in planar lipid bilayers. Ca^{2+} and ATP act as co-agonists of the InsP$_3$R1, but are not able to activate the channels without InsP$_3$ present (first traces). Addition of 2 μM InsP$_3$ to the cis (cytoplasmic) side activates the InsP$_3$R1 (third traces). Current traces at the expanded time scale are shown on the bottom.
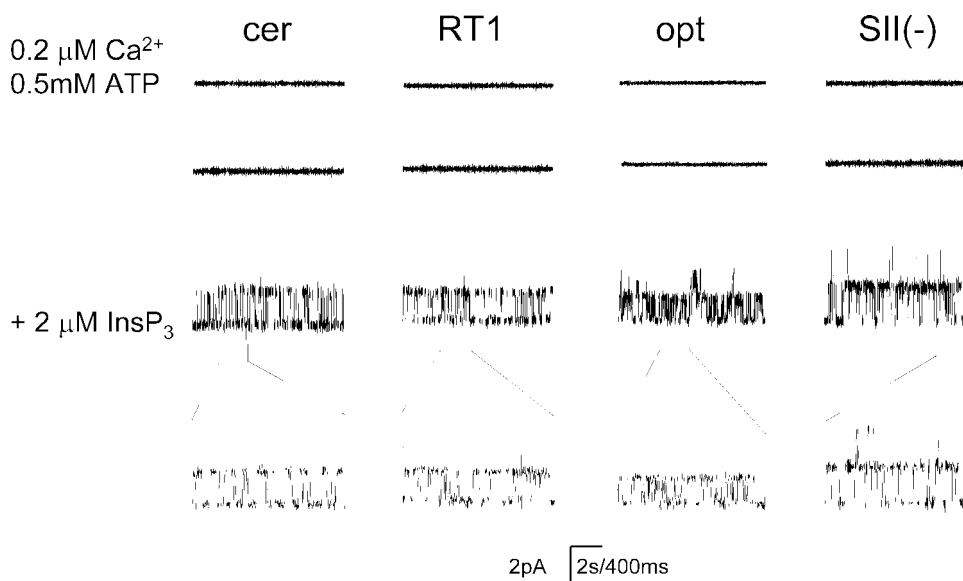
InsP$_3$R1-*opt* mutant channels, we fused microsomes from the Sf9 cells infected with SII(−) and *opt* baculoviruses with planar lipid bilayers. In both cases the InsP$_3$-gated channels were recorded (Fig. 2). The gating behavior of the InsP$_3$R1-SII(−) splice variant and the InsP$_3$R1-*opt* mutant channels was similar to the behavior of InsP$_3$R1-SII(+) and native cerebellar InsP$_3$R, but the unitary current was different (Fig. 2). Indeed, in identical recording conditions the InsP$_3$R-SII(−) channels supported larger current, and the InsP$_3$R1-*opt* channels supported smaller current than the InsP$_3$R-SII(+) channels (Fig. 2).

Gating and conductance properties

Systematic analysis of the InsP$_3$R1 functional properties (Fig. 3, Table 1) revealed that the mean open times of the channels formed by native cerebellar InsP$_3$R, the InsP$_3$R1-SII(+) isoform, and the InsP$_3$R1-*opt* mutant are all close to 5 ms and are not significantly different from one another. Compared with other isoforms, the mean open time of the InsP$_3$R1-SII(−) channels is elevated by 46% to 7.3 ms (Fig. 3, Table 1). The size of the unitary current for native cerebellar InsP$_3$R and the InsP$_3$R1-SII(+) splice variant was 2.0 pA. The size of the unitary current was increased to 2.3 pA for the InsP$_3$R1-SII(+) splice variant and reduced to 1.6 pA for the InsP$_3$R1-*opt* mutant (Fig. 3). Statistical analysis (Table 1) revealed that the unitary current supported by the InsP$_3$R1-SII(−) splice variant is significantly larger and the current supported by the InsP$_3$R1-*opt* mutant is significantly smaller than the current supported by the native cerebellar InsP$_3$R or recombinant InsP$_3$R1-SII(+) isoform.

To further characterize the conductance properties of different InsP$_3$R1 isoforms, we determined the unitary current supported by these channels at various transmembrane potentials between + 10 mV and −30 mV (Fig. 4). The

slope of the resulting current-voltage relationship provided us with the value of single-channel conductance equal to 80 pS for the native cerebellar InsP$_3$R, 81 pS for the InsP$_3$R1-SII(+), 94 pS for the InsP$_3$R1-SII(−), and 64 pS for the InsP$_3$R1-*opt* (Fig. 4, Table 1). Thus, we concluded that the single-channel conductance of the InsP$_3$R1-SII(−) splice variant is significantly higher and the conductance of the InsP$_3$R1-*opt* mutant is significantly lower than the single-channel conductance of native cerebellar InsP$_3$R or the recombinant InsP$_3$R1-SII(+) isoform.

Modulation by cytosolic calcium

Bell-shaped dependence of the InsP$_3$R1 on cytosolic Ca^{2+} (Bezprozvanny et al., 1991; Finch et al., 1991; Iino, 1990) is one of the fundamental InsP$_3$R1 properties responsible for complex spatiotemporal aspects of Ca^{2+} signaling (Berridge, 1993). In the next series of experiments we evaluated the modulation of recombinant rat InsP$_3$R1-SII(+), the InsP$_3$R-SII(−), and the InsP$_3$R1-*opt* mutant by cytosolic Ca^{2+}. In agreement with the behavior of native cerebellar InsP$_3$R ((Bezprozvanny et al., 1991) and Fig. 5, □) and recombinant rat InsP$_3$R1 expressed in HEK-293 and COS cells (Kaznacheyeva et al., 1998; Ramos-Franco et al., 1998a), recombinant InsP$_3$R1-SII(+) expressed in Sf9 cells displays bell-shaped Ca^{2+} dependence with the maximal open probability at 300 nM Ca^{2+} (Fig. 5, ●). The channels formed by the InsP$_3$R1-SII(−) splice isoform (Fig. 5, ○) and by the InsP$_3$R1-*opt* mutant (Fig. 5, ▲) also display bell-shaped Ca^{2+} dependence with the peak at 300 nM Ca^{2+}. The bell-shaped Ca^{2+} dependence of recombinant InsP$_3$R1-SII(+) was wider than the bell-shaped Ca^{2+} dependence of cerebellar InsP$_3$R (Fig. 5) or the bell-shaped Ca^{2+} dependence of InsP$_3$R1 expressed in HEK-293 cells (Kaznacheyeva et al., 1998). In contrast, the bell-shaped
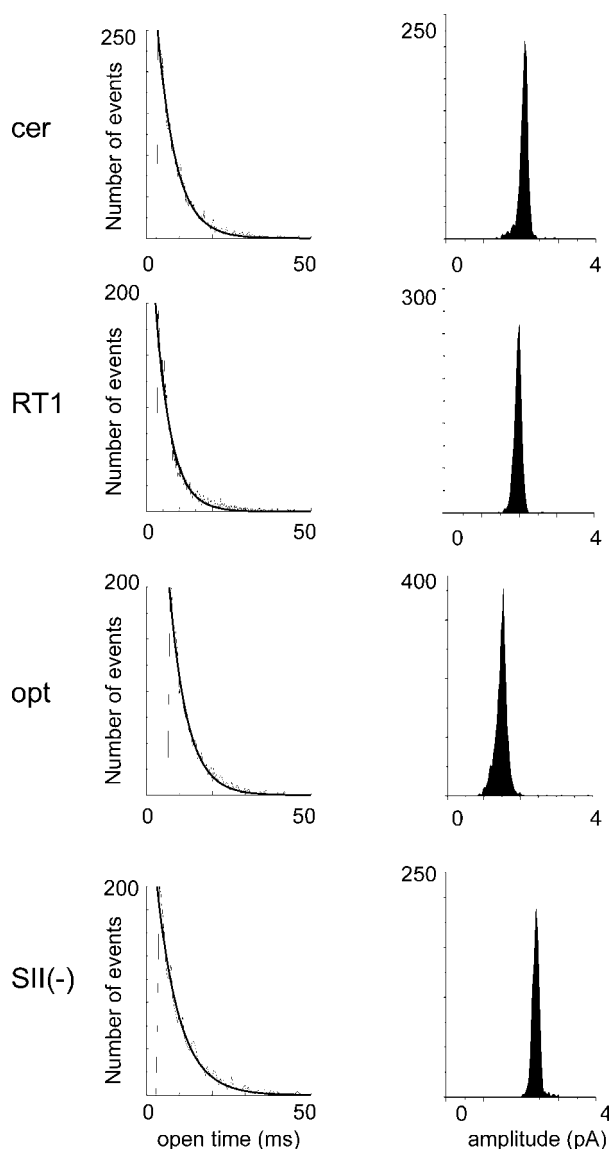
FIGURE 3 Analysis of the single channel records obtained with native rat cerebellar InsP$_3$R (cer), recombinant InsP$_3$R1-SII(+) (RT1), InsP$_3$R1-*opt* (*opt*), and InsP$_3$R1-SII($-$) (SII($-$)) isoforms. Open dwell time (*left*) distributions and unitary current histogram (*right*) are shown. Open time distributions were fit with a single exponential function (*curve*) that yielded τ_0 of 5.5 ms for native rat cerebellar InsP$_3$R, τ_0 of 4.7 ms for InsP$_3$R1-SII(+), τ_0 of 5.2 ms for InsP$_3$R1-*opt*, and τ_0 of 7.3 ms for InsP$_3$R1-SII($-$). Unitary currents were fitted with a Gaussian function that was centered at 2.0 pA for rat cerebellar InsP$_3$R, 1.9 pA for InsP$_3$R1-SII(+), 1.6 pA for InsP$_3$R1-*opt*, and 2.3 pA for InsP$_3$R1-SII($-$). The figure was generated with the data from the same experiments as shown in Fig. 2. Similar analysis of three independent experiments with each InsP$_3$R1 isoform was performed to generate the data presented in Table 1.

Ca^{2+}-dependence of InsP$_3$R1-SII($-$) and InsP$_3$R1-*opt* forms was even narrower than the Ca^{2+}-dependence of native cerebellar InsP$_3$R1 (Fig. 5). To obtain quantitative description of these differences, Ca^{2+}-dependence of different InsP$_3$R1 isoforms was fitted by the bell-shaped equation from (Bezprozvanny et al., 1991) (Fig. 5, smooth curves). The parameters of the optimal Ca^{2+}-dependence fit for all four InsP$_3$R1 isoforms are presented in Table 2. The reasons for the differences in the shape of Ca^{2+}-dependence of different InsP$_3$R1 forms in our experiments are not entirely clear (see Discussion).

To further evaluate the Ca^{2+} regulation of the InsP$_3$R1-SII($-$) splice isoform and the InsP$_3$R1-*opt* mutant form, we compared Ca^{2+} signals induced by B cell receptor stimulation in DT40 cells transfected with the InsP$_3$R1-SII(+), InsP$_3$R1-SII($-$), and InsP$_3$R1-*opt* constructs. The temporal pattern of Ca^{2+} signals in DT40 cells expressing the InsP$_3$R1-SII(+) and InsP$_3$R1-*opt* was indistinguishable (Fig. 6), confirming the conclusion from bilayer experiments that *opt* mutation has only minimal effect on the InsP$_3$R1 modulation by Ca^{2+}. Similar conclusion has been reached in the previous Ca^{2+} imaging studies of Purkinje neurons in *opt* mouse cerebellar slices (Street et al., 1997). A similar response was recorded in DT40 cells expressing InsP$_3$R1-SII($-$) (data not shown). A sensitivity of Ca^{2+} imaging experiments in DT40 cells is not sufficient to detect changes in Ca^{2+} release properties resulting from the described above differences in single-channel conductance between the different InsP$_3$R1 isoforms.

Modulation by ATP

The activity of the InsP$_3$R1 is allosterically potentiated by millimolar concentrations of adenine nucleotides (Bezprozvanny and Ehrlich 1993; Ferris et al., 1990; Iino, 1991). Two ATP-binding sites (ATPA and ATPB) are present in the InsP$_3$R1-SII(+) sequence (Ferris and Snyder, 1992a; Furuichi et al., 1994; Maes et al., 2001, 1999) (Fig. 1 *A*). The ATPA site is deleted in the InsP$_3$R1-*opt* mutant (Fig. 1 *A*). An additional putative ATP-binding site (ATPC) is created in the InsP$_3$R1-SII($-$) splice variant by excision of SII insert (Ferris and Snyder, 1992b) (Fig. 1 *A*). What effect do these changes of the InsP$_3$R1 sequence have on its modulation by ATP? To answer this question, in the next series of experiments we compared the ATP-dependence of recombinant rat InsP$_3$R1-SII(+), the InsP$_3$R1-SII($-$), and the InsP$_3$R1-*opt* mutant. In agreement with the behavior of native cerebellar InsP$_3$R1 ((Bezprozvanny and Ehrlich, 1993); Fig. 7, □), the activity of recombinant InsP$_3$R1-SII(+) expressed in Sf9 cells was allosterically potentiated by ATP with the apparent affinity k_{ATP} of 0.24 mM ATP (Fig. 7, ●). The sensitivity of the InsP$_3$R-*opt* mutant was reduced 20-fold, with the apparent affinity k_{ATP} of 5.3 mM (Fig. 7, ▲). The effect of *opt* mutation on ATP-dependence of InsP$_3$R1 is consistent with the location of the ATPA site in the InsP$_3$R1 sequence (Fig. 1 *A*).

The alternative splicing of SII fragment had a dual effect on ATP-sensitivity of the InsP$_3$R1. First, when compared with the InsP$_3$R1-SII(+) isoform, the apparent affinity for ATP k_{ATP} was reduced sixfold in the InsP$_3$R1-SII($-$) isoform to 1.33 mM (Fig. 7, ○). Second, the InsP$_3$R1-SII($-$)

TABLE 1 Comparison of basic single-channel properties of native rat cerebellar and recombinant InsP$_3$R1-SII(+), InsP$_3$R1-SII(−), and InsP$_3$R1-*opt* forms of the InsP$_3$R1

InsP$_3$R1	Open time τ_o (ms)	Current i (pA)	Conductance γ (pS)	Peak Ca^{2+} (pCa)	k_{ATP} (mM)	$P_\phi/(P_\phi + P_m)$
Cer InsP$_3$R	5.5 ± 0.2	2.02 ± 0.04	80.0 ± 0.1	6.71	0.26	0.01
InsP$_3$R1-SII(+)	4.7 ± 0.6	1.88 ± 0.07	81.0 ± 0.4	6.59	0.24	0.19
InsP$_3$R1-SII(−)	7.3 ± 0.5	2.30 ± 0.03	94.0 ± 0.2	6.72	1.33	0.27
InsP$_3$R1-*opt*	5.2 ± 1.7	1.61 ± 0.01	64.0 ± 0.5	6.72	5.3	0.07

channels were twofold more active than InsP$_3$R1-SII(+) channels in the absence of ATP. On average, at 0 ATP P_o of the InsP$_3$R1-SII(+) channels was 6 ± 2% ($n = 3$), and P_o of the InsP$_3$R1-SII(−) channels was 13 ± 2% ($n = 3$). Similar conclusion was apparent from fitting the ATP-dependence data (Fig. 7, ○); the ratio of P_o in the absence of ATP (P_ϕ) to maximal P_o predicted by the ATP-dependence equation ($P_\phi + P_m$) is 0.19 for the InsP$_3$R1-SII(+) isoform and 0.27 for the InsP$_3$R1-SII(−) isoform (Table 1).

DISCUSSION

In this paper we compared the main functional properties of native rat cerebellar InsP$_3$R1, recombinant rat InsP$_3$R1-SII(+) and InsP$_3$R1-SII(−) splice variants, and recombinant InsP$_3$R1-*opt* deletion mutant. The properties of the channels were analyzed using planar lipid bilayer technique in identical experimental conditions. Recombinant InsP$_3$R1 for these studies were expressed in Sf9 cells using baculovirus-mediated infection. From obtained results we concluded that: 1) the properties of recombinant InsP$_3$R1-SII(+) channels expressed in Sf9 cells follow most of the

properties of the native cerebellar InsP$_3$R1; 2) the InsP$_3$R1-SII(−) splice variant has higher conductance (94 pS) and the InsP$_3$R1-*opt* mutant has lower conductance (64 pS) than the InsP$_3$R1-SII(+) isoform (81 pS); 3) the mean open channel time is ~5 ms for the InsP$_3$R1-SII(+) and InsP$_3$R1-*opt* isoforms and 7.3 ms for the InsP$_3$R1-SII(−) isoform; 4) all three InsP$_3$R1 isoforms display bell-shaped Ca^{2+}-dependence on cytosolic Ca^{2+} with the peak at 200–300 nM Ca^{2+}; 5) the bell-shaped Ca^{2+}-dependence is wider for the InsP$_3$R1-SII(+) isoform when compared with the InsP$_3$R1-SII(−) and InsP$_3$R1-*opt* isoforms, indicating possible differences in cooperative interaction between InsP$_3$R1 subunits; 6) all three InsP$_3$R1 isoforms support similar pattern of Ca^{2+} signals when expressed in DT40 cells; 7) when

FIGURE 5 Bell-shaped Ca^{2+} dependence of native rat cerebellar InsP$_3$R (cer), recombinant InsP$_3$R1-SII(+) (RT1), InsP$_3$R1-*opt* (*opt*), and InsP$_3$R1-SII(−) (SII(−)) isoforms. The open-channel probability of the InsP$_3$R1 (P_o) was determined in the presence of 2 μM InsP$_3$, 0.5 mM Na$_2$ATP, and the *cis* (cytosolic) Ca^{2+} concentrations in the range between 10 nM and 5 μM Ca^{2+}. P_0 in each experiment was normalized to maximum P_0 observed in the same experiment, and then data from several independent experiments were averaged together at each Ca^{2+} concentration. The normalized and averaged data at each Ca^{2+} concentration are shown as mean ± SE ($n \geq 3$) for rat cerebellar InsP$_3$R (□), InsP$_3$R1-SII(+) (●), InsP$_3$R1-*opt* (▲), and InsP$_3$R1-SII(−) (○). These data were fitted by the bell-shaped equation $P(Ca^{2+}) = P_m\,k^n[Ca^{2+}]^n/((k^n + [Ca^{2+}]^n)(K^n + [Ca^{2+}]^n))$ from Bezprozvanny et al. (1991), where n is a Hill coefficient, k is the apparent affinity of Ca^{2+} activating site, and K is the apparent affinity of Ca^{2+} inhibitory site. The parameters of the best fit (*smooth curves*) are presented in Table 2.
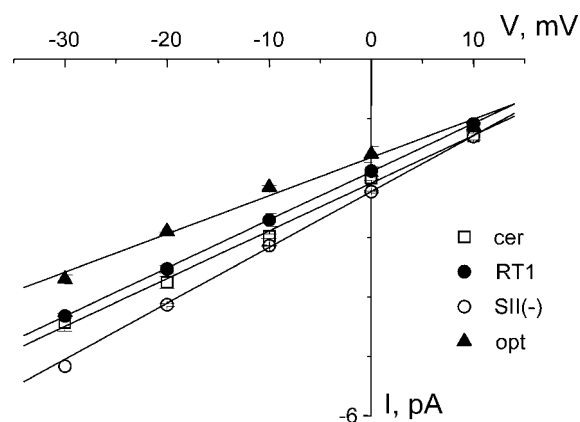

FIGURE 4 Current-voltage relationship of native rat cerebellar InsP$_3$R (cer), recombinant InsP$_3$R1-SII(+) (RT1), InsP$_3$R1-*opt* (*opt*), and InsP$_3$R1-SII(−) (SII(−)) isoforms. Activities of these InsP$_3$R1 isoforms were recorded in planar lipid bilayers in the range of transmembrane potentials from −30 mV to +10 mV. Single-channel current amplitude at each voltage was determined from a Gaussian fit. The data sets were fit by a linear regression ($r = 0.99$) with a slope of 80 pS for cerebellar InsP$_3$R (□), 81 pS for InsP$_3$R-SII(+) (●), 64 pS for InsP$_3$R1-*opt* (▲), and 94 pS for InsP$_3$R1-SII(−) (○). All points represented mean (±SE; $n \geq 3$).
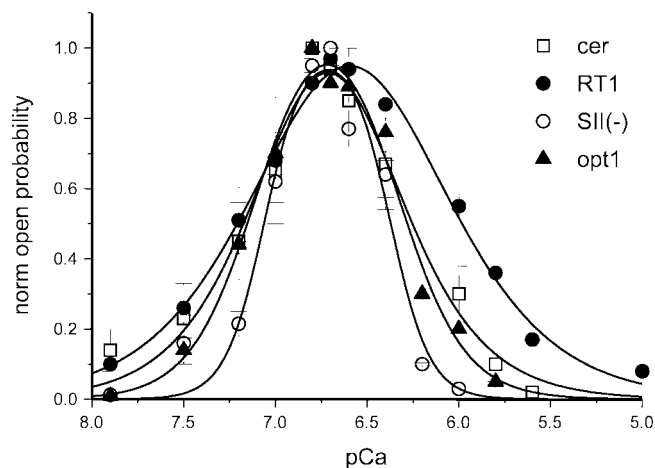
TABLE 2   Parameters of bell-shaped fit to the Ca²⁺-dependence data obtained with the rat cerebellar InsP₃R1 and recombinant InsP₃R1-SII(+), InsP₃R1-SII(−), and InsP₃R1-*opt* isoforms

InsP₃R1	Hill coefficient n	Affinity of the activating site k (μM)	Affinity of the inhibitory site K (μM)	Peak of Ca²⁺ dependence (pCa)
Cer InsP₃R	1.56	0.20	0.19	6.71
InsP₃R1-SII(+)	1.22	0.37	0.17	6.59
InsP₃R1-SII(−)	4.04	0.42	0.09	6.72
InsP₃R1-*opt*	2.37	0.45	0.08	6.72

compared with the InsP₃R1-SII(+) isoform, the sensitivity to modulation by ATP is 20-fold lower in the InsP₃R1-*opt* mutant and sixfold lower in the InsP₃R1-SII(−) splice variant; 8) when compared with InsP₃R1-SII(+), the activity of InsP₃R1-SII(−) in the absence of ATP is elevated twofold. The main results of this paper are summarized in Table 1 and briefly discussed below.

Our finding that an alternative splicing (SII) or deletion (*opt*) in the coupling domain has an effect on single-channel conductance of the InsP₃R1 was unexpected. According to the conventional model of the InsP₃R domain structure, the structural determinants of channel pore are localized to the carboxy-terminal Ca²⁺ channel domain (Mignery and Sudhof, 1990; Miyawaki et al., 1991). From our results it seems that the middle portion of the coupling domain is intimately involved in the function of the InsP₃R pore. The amino-

terminal and carboxy-terminal regions of InsP₃R have been shown to associate directly in biochemical experiments (Boehning and Joseph, 2000a; Joseph et al., 1995), and it is possible that the middle portion of the coupling domain is localized in the proximity of the channel pore in the three-dimensional structure of the InsP₃R. Interestingly, the effect of SII splicing on channel conductance seems more pronounced when divalent cations are used as current carrier. In our experiments with 50 mM Ba²⁺ as a current carrier, the single channel conductance of the InsP₃R1-SII(−) isoform was elevated by 16% (94 pS for SII(−) versus 81 pS for SII(+) (Fig. 4), whereas in experiments of Boehning et al. (2001) with 140 mM K⁺, the difference between single-channel conductance values of InsP₃R1-SII splice variants was only 5% (390 pS for SII(−) vs 370 pS for SII(+)). Changes in InsP₃R1 conductance induced by SII splicing event are not likely to be associated with the change in the InsP₃R1 PKA-phosphorylation pattern (Danoff et al., 1991; Ferris et al., 1991a) (Fig. 1 *A*). In an independent series of experiments we established that only ~20% of the InsP₃R1 expressed in Sf9 cells are in the PKA-phosphorylated state and that the single channel conductance of the InsP₃R1-SII(+) channels is not influenced by PKA phosphorylation (Tang at al, submitted for publication).

We concluded that the peak of bell-shaped Ca²⁺-dependence located at pCa 6.6–6.7 for the InsP₃R1-SII(+), InsP₃R1-SII(−), and InsP₃R1-*opt* (Fig. 5, Tables 1 and 2). In agreement with this finding, the smooth muscle cells expressing the InsP₃R-SII(−) isoform display Ca²⁺ depen-
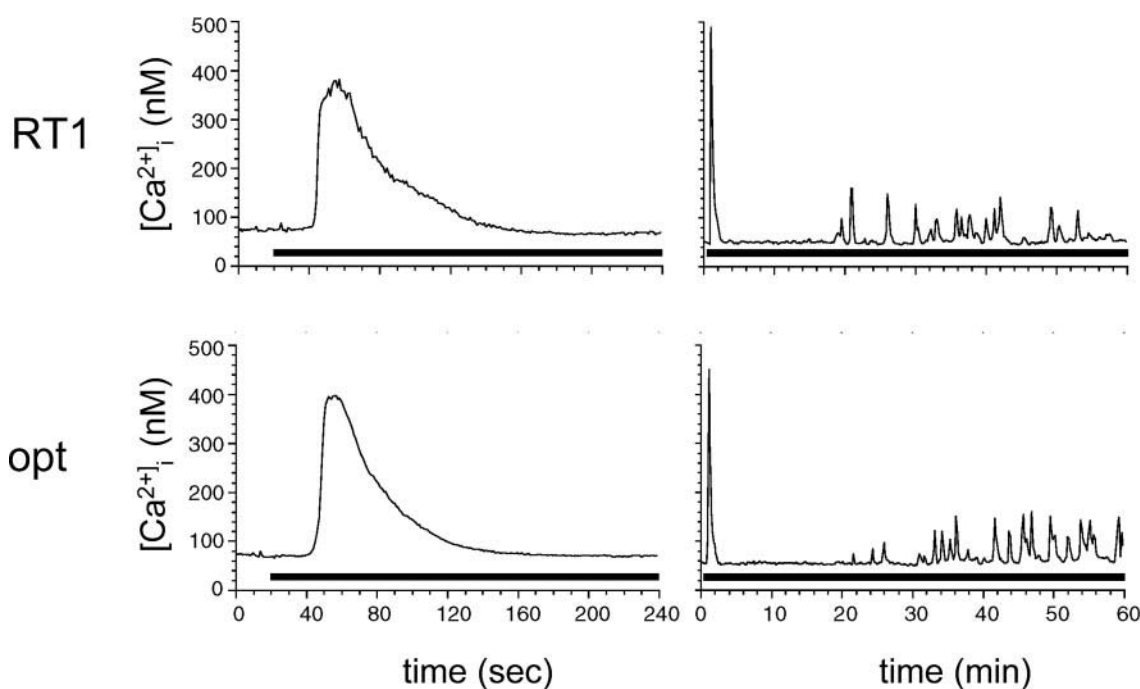

FIGURE 6   Ca²⁺ signals in DT40 cells expressing InsP₃R1-SII(+) (RT1) and InsP₃R1-*opt* (*opt*) in response to BCR stimulation. The data are shown for 4 min (*left*) and 60 min (*right*). The anti-BCR antibody (1 μg/ml) was applied as indicated by the horizontal bars below the traces.
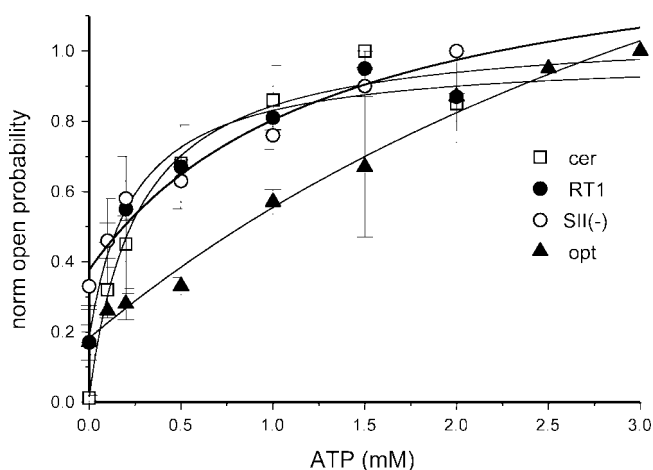
FIGURE 7 Allosteric potentiation of native rat cerebellar InsP$_3$R (cer), and recombinant InsP$_3$R1-SII(+) (RT1), InsP$_3$R1-*opt* (*opt*), and InsP$_3$R1-SII(−)(SII(−)) isoforms by ATP. The single-channel open probability was measured as a function of Na$_2$ATP concentration on the cytoplasmic side of the membrane. The ATP concentration ranged from 0 to 3.0 mM. At least 100 s of continuous recording at each concentration for ATP were analyzed to obtain the open probability. The open probability was normalized to the maximal open probability observed in the same experiment. The normalized data from several experiments with each InsP$_3$R1 isoform were averaged together and plotted as mean ± SE ($n \geq 3$) for native cerebellar InsP$_3$R (□), InsP$_3$R1-SII(+) (●), InsP$_3$R1-*opt* (▲), and InsP$_3$R1-SII(−) (○). The data were fit by the equation $P([ATP]) = P_\phi + P_m[ATP]/(k_{ATP} + [ATP])$ from Bezprozvanny and Ehrlich (1993), where P_ϕ is the open probability in the absence of ATP, P_m is the maximal increase in P_o induced by ATP, and k_{ATP} is the apparent affinity for ATP. The parameters of the best fit (*smooth curves*) are in Table 1.

dence of InsP$_3$-induced Ca^{2+} release with the maximum at pCa 6.5 (Iino, 1990), similar to the cerebellar InsP$_3$R1-SII(+) isoform with the maximim at pCa 6.7 (Bezprozvanny et al., 1991). Using a Ca^{2+} flux assay with transfected COS cells, Boehning and Joseph (2000b) reported that the InsP$_3$R1-SII(−) isoform is significantly more sensitive to modulation by Ca^{2+} than InsP$_3$R1-SII(+), with the peak at 10–20 nM Ca^{2+} (pCa 8). However, the same group reported similar Ca^{2+} dependence of InsP$_3$R1-SII(−) and InsP$_3$R1-SII(+) isoforms in patch-clamp studies of InsP$_3$R expressed in a COS cell nuclear envelope (Boehning et al., 2001). Thus, most likely the discrepancy between our results and the data of Boehning and Joseph (2000) is caused by the difference in assays used to analyze the recombinant InsP$_3$R1-SII(−) function.

Although the peak of Ca^{2+}-dependence was observed at pCa 6.6−6.7 for all InsP$_3$R1 isoforms tested in our study, the shape of Ca^{2+}-dependence bell was wider for the InsP$_3$R1-SII(+) than for the InsP$_3$R1-SII(−) and InsP$_3$R1-*opt* isoforms (Fig. 5). Also, the Ca^{2+}-dependence was wider for the InsP$_3$R1-SII(+) than for the native cerebellar InsP$_3$R1 (Fig. 5). To obtain quantitative description of these differences, Ca^{2+}-dependence of different InsP$_3$R1 isoforms was fitted by the bell-shaped equation from (Bez-

prozvanny et al., 1991) (Fig. 5, smooth curves). The fitting procedure yielded Hill coefficient (n) of 1.56 for cerebellar InsP$_3$R, 1.22 for InsP$_3$R1-SII(+), 4.04 for InsP$_3$R1-SII(−), and 2.37 for InsP$_3$R1-*opt* (Table 2). At the moment, we do not clearly understand the reasons for observed differences in the width of bell-shaped Ca^{2+} dependence, but it is possible that alternative splicing (SII-) or deletion (*opt*) in the InsP$_3$R1 coupling domain affects interactions between InsP$_3$R1 subunits. The reasons for the differences in the width of Ca^{2+}-dependence of the InsP$_3$R1-SII(+) expressed in Sf9 cells and of the native cerebellar InsP$_3$R (Fig. 5) or InsP$_3$R1-SII(+) expressed in HEK-293 cells (Kaznacheyeva et al., 1998) are also not clear. The most likely possibility is related to the absence of an auxiliary protein, such as FKBP12, in Sf9 cells (Brillantes et al., 1994). Future studies will be required to clarify this issue. Parameters of our fitting procedure indicate that the apparent affinity of Ca^{2+}-activating site is close to 0.4 μM Ca^{2+} for all 3 InsP$_3$R1 isoforms (Table 2), in agreement with location of the InsP$_3$R1 Ca^{2+} sensor region (Miyakawa et al., 2001) outside the area affected by SII splicing and *opt* mutation (Fig. 1 *A*). When compared with InsP$_3$R1-SII(+), the apparent affinity of Ca^{2+}-inhibitory site is elevated twofold in InsP$_3$R1-SII(−) and InsP$_3$R1-*opt* isoforms (Table 2). Thus, a putative Ca^{2+}-inhibitory site may be located close to the region affected by SII splicing and *opt* mutation.

The dramatic effect of *opt* mutation on ATP-dependence of InsP$_3$R1 is consistent with the location of the ATPA site in the InsP$_3$R1 sequence (Fig. 1 *A*). In our experiments the apparent affinity for potentiation by ATP is reduced 20-fold in the InsP$_3$R1-*opt* mutant (Fig. 7, Table 1). The remaining sensitivity to ATP modulation in the InsP$_3$R-*opt* mutant is likely to be conferred by the intact ATPB site (Fig. 1 *A*). Notably, the ATPA site is unique for the InsP$_3$R1 isoform, whereas the ATPB site is conserved among InsP$_3$R1, InsP$_3$R2, and InsP$_3$R3 isoforms (Furuichi et al., 1994). When InsP$_3$R1 and InsP$_3$R3 isoforms were compared in Ca^{2+} flux studies, at least 10-fold reduction in sensitivity to ATP modulation has been observed for the InsP$_3$R3 isoform (Maes et al., 2000; Missiaen et al., 1998; Miyakawa et al., 1999). Thus, our data with the InsP$_3$R1-*opt* mutant support the notion that the ATPA site is responsible for high-affinity ATP binding and the affinity of the ATPB site is at least 10-fold lower (Maes et al., 2001).

The effect of SII splicing on ATP sensitivity is more complex. The apparent affinity to ATP potentiation is reduced approximately sixfold in the nonneuronal InsP$_3$R1-SII(−) isoform (Fig. 7, Table 1). In contrast, a level of basal activity in the absence of ATP is elevated twofold for the InsP$_3$R1-SII(−) isoform (Fig. 7, Table 1). In principle, our data agree with the previous description of the adenine nucleotide effect on InsP$_3$-induced Ca^{2+} release in smooth muscle cells (Iino, 1991), but detailed quantitative comparison is difficult. The ATPA site is intact in InsP$_3$R1-SII(−) isoform (Fig. 1 *A*), and the observed changes is likely to be

attributable to overall changes in the InsP$_3$R1 coupling domain conformation induced by the SII splicing event. It is also possible that an additional ATPC site created in InsP$_3$R1-SII($-$) isoform by SII excision (Ferris and Snyder, 1992b) (Fig. 1 *A*) is inhibitory, leading to reduction in the apparent affinity of InsP$_3$R1 for ATP.

Our data provide some new information related to the *opisthotonos* mouse phenotype. In agreement with conclusions of Street et al. (1997), we established that the InsP$_3$R1 containing the *opt* mutation is functional. The major cause of the *opisthotonos* phenotype is likely to be an impairment of Ca^{2+} release from intracellular stores resulting from a 10-fold reduction in level of the InsP$_3$R1 protein in the brain of *opisthotonos* mouse (Street et al., 1997). Interestingly, the InsP$_3$R1-*opt* mutant expressed in Sf9 cells seems to be more prone to proteolysis than the wild-type InsP$_3$R1 isoforms (Fig. 1 *B*). It is possible that the increased sensitivity of InsP$_3$R1-*opt* mutant to proteolysis is linked to reduction in the level of the InsP$_3$R1 protein in the brain of the *opt* mutant mice (Street et al., 1997). In addition, we found that when compared with the wild-type InsP$_3$R1-SII($+$), the single-channel conductance of the InsP$_3$R1-*opt* mutant is reduced by 20% (Fig. 4) and sensitivity to potentiation by ATP is reduced 20-fold (Fig. 7). These changes in InsP$_3$R1 properties did not have a significant effect on BCR response when InsP$_3$R1-*opt* mutant was expressed and tested in DT40 cells (Fig. 6) but, in the brain, alterations in InsP$_3$R1 properties may contribute to severity of the *opisthotonos* mouse phenotype.

REFERENCES

Berridge, M. J. 1993. Inositol trisphosphate and calcium signalling. *Nature.* 361:315–325.

Bezprozvanny, I., and B. E. Ehrlich. 1993. ATP modulates the function of inositol 1,4,5-trisphosphate-gated channels at two sites. *Neuron.* 10:1175–1184.

Bezprozvanny, I., and B. E. Ehrlich. 1994. Inositol (1, 4, 5)-trisphosphate (InsP$_3$)-gated Ca channels from cerebellum: conduction properties for divalent cations and regulation by intraluminal calcium. *J. Gen. Physiol.* 104:821–856.

Bezprozvanny, I., and B. E. Ehrlich. 1995. The inositol 1,4,5-trisphosphate (InsP$_3$) receptor. *J. Membr. Biol.* 145:205–216.

Bezprozvanny, I., J. Watras, and B. E. Ehrlich. 1991. Bell-shaped calcium-response curves of Ins(1, 4, 5)P$_3$- and calcium-gated channels from endoplasmic reticulum of cerebellum. *Nature.* 351:751–754.

Boehning, D., and S. K. Joseph. 2000a. Direct association of ligand-binding and pore domains in homo- and heterotetrameric inositol 1,4,5-trisphosphate receptors. *EMBO J.* 19:5450–5459.

Boehning, D., and S. K. Joseph. 2000b. Functional properties of recombinant type I and type III inositol 1, 4, 5-trisphosphate receptor isoforms expressed in COS-7 cells. *J. Biol. Chem.* 275:21492–21499.

Boehning, D., S. K. Joseph, D. O. Mak, and J. K. Foskett. 2001. Single-channel recordings of recombinant inositol trisphosphate receptors in mammalian nuclear envelope. *Biophys. J.* 81:117–124.

Brillantes, A. B., K. Ondrias, A. Scott, E. Kobrinsky, E. Ondriasova, M. C. Moschella, T. Jayaraman, M. Landers, B. E. Ehrlich, and A. R. Marks. 1994. Stabilization of calcium release channel (ryanodine receptor) function by FK506-binding protein. *Cell.* 77:513–523.

Cameron, A. M., J. P. Steiner, A. J. Roskams, S. M. Ali, G. V. Ronnett, and S. H. Snyder. 1995. Calcineurin associated with the inositol 1,4,5-trisphosphate receptor-FKBP12 complex modulates Ca^{2+} flux. *Cell.* 83:463–472.

Colquhoun, D., and A. G. Hawkes. 1995. The principle of the stochastic interpretation of ion-channel mechanisms. In: Single Channel Recording, 2nd ed. B. Sakmann and E. Neher, editors. Plenum Publishing, New York. 397–482.

Danoff, S. K., C. D. Ferris, C. Donath, G. A. Fischer, S. Munemitsu, A. Ullrich, S. H. Snyder, and C. A. Ross. 1991. Inositol 1,4,5-trisphosphate receptors: distinct neuronal and nonneuronal forms derived by alternative splicing differ in phosphorylation. *Proc. Natl. Acad. Sci. U.S.A.* 88:2951–2955.

Fabiato, A. 1988. Computer programs for calculating total from specified free or free from specified total ionic concentrations in aqueous solutions containing multiple metals and ligands. *Methods Enzymol.* 157:378–417.

Ferris, C. D., A. M. Cameron, D. S. Bredt, R. L. Huganir, and S. H. Snyder. 1991a. Inositol 1,4,5-trisphosphate receptor is phosphorylated by cyclic AMP-dependent protein kinase at serines 1755 and 1589. *Biochem. Biophys. Res. Commun.* 175:192–198.

Ferris, C. D., R. L. Huganir, D. S. Bredt, A. M. Cameron, and S. H. Snyder. 1991b. Inositol trisphosphate receptor-phosphorylation by protein kinase-C and calcium calmodulin-dependent protein kinases in reconstituted lipid vesicles. *Proc. Natl. Acad. Sci. U.S.A.* 88:2232–2235.

Ferris, C. D., R. L. Huganir, and S. H. Snyder. 1990. Calcium flux mediated by purified inositol 1,4,5-trisphosphate receptor in reconstituted lipid vesicles is allosterically regulated by adenine nucleotides. *Proc. Natl. Acad. Sci. U.S.A.* 87:2147–2151.

Ferris, C. D., and S. H. Snyder. 1992a. Inositol 1:4.,5-trisphosphate-activated calcium channels. *Annu. Rev. Physiol.* 54:469–488.

Ferris, C. D., and S. H. Snyder. 1992b. Inositol phosphate receptors and calcium disposition in the brain. *J. Neurosci.* 12:1567–1574.

Finch, E. A., T. J. Turner, and S. M. Goldin. 1991. Calcium as a coagonist of inositol 1,4,5-trisphosphate-induced calcium release. *Science.* 252:443–446.

Fujii, S., M. Matsumoto, K. Igarashi, H. Kato, and K. Mikoshiba. 2000. Synaptic plasticity in hippocampal CA1 neurons of mice lacking type 1 inositol-1,4,5-trisphosphate receptors. *Learn. Mem.* 7:312–320.

Furuichi, T., K. Kohda, A. Miyawaki, and K. Mikoshiba. 1994. Intracellular channels. *Curr. Opin. Neurobiol.* 4:294–303.

Grynkiewicz, G., M. Poenie, and R. Y. Tsien. 1985. A new generation of Ca^{2+} indicators with greatly improved fluorescence properties. *J. Biol. Chem.* 260:3440–3450.

Horn, R. 1991. Estimating the number of channels in patch recordings. *Biophys. J.* 60:433–439.

Iino, M. 1990. Biphasic Ca^{2+} dependence of inositol 1,4,5-trisphosphate-induced Ca release in smooth muscle cells of the guinea pig *Taenia caeci.* *J. Gen. Physiol.* 95:1103–1122.

Iino, M. 1991. Effects of adenine nucleotides on inositol 1,4,5-trisphosphate-induced calcium release in vascular smooth muscle cells. *J. Gen. Physiol.* 98:681–698.

Islam, M. O., Y. Yoshida, T. Koga, M. Kojima, K. Kangawa, and S. Imai. 1996. Isolation and characterization of vascular smooth muscle inositol 1,4,5-trisphosphate receptor. *Biochem. J.* 316:295–302.

Itoh, S., K. Ito, S. Fujii, K. Kaneko, K. Kato, K. Mikoshiba, and H. Kato. 2001. Neuronal plasticity in hippocampal mossy fiber-CA3 synapses of

mice lacking the inositol-1,4,5-trisphosphate type 1 receptor. *Brain Res.* 901:237–246.

Joseph, S. K., S. Pierson, and S. Samanta. 1995. Trypsin digestion of the inositol trisphosphate receptor: implications for the conformation and domain organization of the protein. *Biochem. J.* 307:859–865.

Kaznacheyeva, E., V. D. Lupu, and I. Bezprozvanny. 1998. Single-channel properties of inositol (1,4,5)-trisphosphate receptor heterologously expressed in HEK-293 cells. *J. Gen. Physiol.* 111:847–856.

Lin, C., J. Widjaja, and S. K. Joseph. 2000. The interaction of calmodulin with alternatively spliced isoforms of the type-I inositol trisphosphate receptor. *J. Biol. Chem.* 275:2305–2311.

Maeda, N., T. Kawasaki, S. Nakade, N. Yokota, T. Taguchi, M. Kasai, and K. Mikoshiba. 1991. Structural and functional characterization of inositol 1,4,5-trisphosphate receptor channel from mouse cerebellum. *J. Biol. Chem.* 266:1109–1116.

Maes, K., L. Missiaen, P. De Smet, S. Vanlingen, G. Callewaert, J. B. Parys, and H. De Smedt. 2000. Differential modulation of inositol 1,4,5-trisphosphate receptor type 1 and type 3 by ATP. *Cell. Calcium.* 27:257–267.

Maes, K., L. Missiaen, J. B. Parys, P. De Smet, I. Sienaert, E. Waelkens, G. Callewaert, and H. De Smedt. 2001. Mapping of the ATP-binding sites on inositol 1,4,5-trisphosphate receptor type 1 and type 3 homotetramers by controlled proteolysis and photoaffinity labeling. *J. Biol. Chem.* 276:3492–3497.

Maes, K., L. Missiaen, J. B. Parys, I. Sienaert, G. Bultynck, M. Zizi, P. De Smet, R. Casteels, and H. De Smedt. 1999. Adenine-nucleotide binding sites on the inositol 1,4,5-trisphosphate receptor bind caffeine, but not adenophostin A or cyclic ADP-ribose. *Cell. Calcium.* 25:143–152.

Matsumoto, M., T. Nakagawa, T. Inoue, E. Nagata, K. Tanaka, H. Takano, O. Minowa, J. Kuno, S. Sakakibara, M. Yamada, H. Yoneshima, A. Miyawaki, Y. Fukuuchi, T. Furuichi, H. Okano, K. Mikoshiba, and T. Noda. 1996. Ataxia and epileptic seizures in mice lacking type 1 inositol 1,4,5-trisphosphate receptor. *Nature.* 379:168–171.

Mignery, G., T. C. Sudhof, K. Takei, and P. De Camilli. 1989. Putative receptor for inositol 1,4,5-trisphosphate similar to ryanodine receptor. *Nature.* 342:192–195.

Mignery, G. A., C. L. Newton, B. T. Archer, and T. C. Sudhof. 1990. Structure and expression of the rat inositol 1,4,5-trisphosphate receptor. *J. Biol. Chem.* 265:12679–12685.

Mignery, G. A., and T. C. Sudhof. 1990. The ligand binding site and transduction mechanism in the inositol-1,4,5-triphosphate receptor. *EMBO J.* 9:3893–3898.

Missiaen, L., J. B. Parys, I. Sienaert, K. Maes, K. Kunzelmann, M. Takahashi, K. Tanzawa, and H. De Smedt. 1998. Functional properties of the type-3 InsP3 receptor in 16HBE14o- bronchial mucosal cells. *J. Biol. Chem.* 273:8983–8986.

Miyakawa, T., A. Maeda, T. Yamazawa, K. Hirose, T. Kurosaki, and M. Iino. 1999. Encoding of Ca^{2+} signals by differential expression of IP3 receptor subtypes. *EMBO J.* 18:1303–1308.

Miyakawa, T., A. Mizushima, K. Hirose, T. Yamazawa, I. Bezprozvanny, T. Kurosaki, and M. Iino. 2001. Ca^{2+}-sensor region of IP(3) receptor controls intracellular Ca^{2+} signaling. *EMBO J.* 20:1674–1680.

Miyawaki, A., T. Furuichi, Y. Ryou, S. Yoshikawa, T. Nakagawa, T. Saitoh, and K. Mikoshiba. 1991. Structure-function relationships of the mouse inositol 1,4,5-trisphosphate receptor. *Proc. Natl. Acad. Sci. U.S.A.* 88:4911–4915.

Nakade, S., S. K. Rhee, H. Hamanaka, and K. Mikoshiba. 1994. Cyclic AMP-dependent phosphorylation of an immunoaffinity-purified homotetrameric inositol 1,4,5-trisphosphate receptor (type I) increases Ca^{2+} flux in reconstituted vesicles. *J. Biol. Chem.* 269:6735–6742.

Nakagawa, T., H. Okano, T. Furuichi, J. Aruga, and K. Mikoshiba. 1991a. The subtypes of the mouse inositol 1,4,5-trisphosphate receptor are expressed in a tissue-specific and developmentally specific manner. *Proc. Natl. Acad. Sci. U.S.A.* 88:6244–6248.

Nakagawa, T., C. Shiota, H. Okano, and K. Mikoshiba. 1991b. Differential localization of alternative spliced transcripts encoding inositol 1,4,5-trisphosphate receptors in mouse cerebellum and hippocampus: in situ hybridization study. *J. Neurochem.* 57:1807–1810.

Ramos-Franco, J., S. Caenepeel, M. Fill, and G. Mignery. 1998a. Single channel function of recombinant type-1 inositol 1,4,5-trisphosphate receptor ligand binding domain splice variants. *Biophys. J.* 75:2783–2793.

Ramos-Franco, J., M. Fill, and G. A. Mignery. 1998b. Isoform-specific function of single inositol 1,4,5-trisphosphate receptor channels. *Biophys. J.* 75:834–839.

Street, V. A., M. M. Bosma, V. P. Demas, M. R. Regan, D. D. Lin, L. C. Robinson, W. S. Agnew, and B. L. Tempel. 1997. The type 1 inositol 1,4,5-trisphosphate receptor gene is altered in the opisthotonos mouse. *J. Neurosci.* 17:635–645.

Sugawara, H., M. Kurosaki, M. Takata, and T. Kurosaki. 1997. Genetic evidence for involvement of type 1, type 2 and type 3 inositol 1,4,5-trisphosphate receptors in signal transduction through the B-cell antigen receptor. *EMBO J.* 16:3078–3088.

Supattapone, S., S. K. Danoff, A. Theibert, S. K. Joseph, J. Steiner, and S. H. Snyder. 1988. Cyclic AMP-dependent phosphorylation of a brain inositol trisphosphate receptor decreases its release of calcium. *Proc. Natl. Acad. Sci. U.S.A.* 85:8747–8750.

Taylor, C. W. 1998. Inositol trisphosphate receptors: Ca^{2+}-modulated intracellular Ca^{2+} channels. *Biochim. Biophys. Acta.* 1436:19–33.

Yamamoto, H., N. Maeda, M. Niinobe, E. Miyamoto, and K. Mikoshiba. 1989. Phosporylation of P400 protein by cyclic AMP-dependent protein kinase and Ca/calmodulin-dependent protein kinase II. *J. Neurochem.* 53:917–923.